Available online at www.CivileJournal.org

# Civil Engineering Journal

(E-ISSN: 2476-3055; ISSN: 2676-6957)

Vol. 10, No. 07, July, 2024


# Effectiveness of Grouting and GFRP Reinforcement for Repairing Spalled Reinforced Concrete Beams

Achmad Z. Mansur [1*], Rudy Djamaluddin [2], Herman Parung [2], Rita Irmawaty [2], Daud Nawir [1]

[1] *Department of Civil Engineering, Faculty of Engineering, Borneo Tarakan University, North Kalimantan 77115, Indonesia.*

[2] *Department of Civil Engineering, Faculty of Engineering, Hasanuddin University, South Sulawesi 91711, Indonesia.*

Received 05 February 2024; Revised 02 June 2024; Accepted 09 June 2024; Published 01 July 2024

**Abstract**

Corrosion of steel reinforcement from chloride exposure can compromise the strength of reinforced concrete structures. Rust formation expands, applying pressure on concrete, resulting in cracks and spalling. Prompt repair is crucial for severe cases of spalling. This research assessed the efficacy of repair strategies for reinforced concrete beams post-spalling, including grouting and different techniques involving Glass Fiber Reinforced Polymer (GFRP) reinforcement. The research examined four variations of reinforced concrete beams, each sized at 150 mm × 200 mm × 3300 mm. Results showed that the standard beam (BK) had an average maximum load capacity of 29.74 kN. In contrast, the grouted beam (BGR) demonstrated a reduced maximum load of 14.39 kN, along with decreased steel and concrete strain compared to BK. This suggests that the grouting repair did not fully restore the beam's flexural capacity after spalling. Incorporating GFRP strips (BGRS) led to a marginal increase in the beam's maximum load, albeit remaining below BK, with lower steel and concrete strain than BK. However, the steel and concrete approached their yield points, indicating enhanced flexural performance. The full-wrap GFRP beam (BGRSF) experienced an 8.08% increase in maximum load compared to BK, with concrete strain surpassing BK, suggesting an enhancement in flexural stiffness.

*Keywords:* RC Beam; Spalling; Sikagrout-215; GFRP Sheet.

## 1. Introduction

Rafters play a pivotal role as the main structural components of bridges, ensuring an even distribution of the bridge's load. Usually constructed from steel or reinforced concrete, girders are engineered to withstand various applied loads. Nonetheless, despite their resilience, girders remain prone to corrosion triggered by exposure to water, air, or corrosive substances. This corrosion, termed spalling when it affects bridge girders, can inflict damage on the concrete surface. Spalling manifests when the concrete layer encasing the girder flakes or fractures due to the pressure exerted by the expanded volume of oxide exceeding the original metal volume [1]. Chloride attack frequently triggers the corrosion of girders, especially in harsh environments like coastal regions or areas with significant pollution. This type of attack happens when dissolved salts, like seawater or salt-contaminated water, infiltrate the girder through cracks or compromise its protective layer [2]. These salts harbor extremely corrosive chloride ions, capable of undermining the passive protection on the metal surface and accelerating the corrosion process. Safeguarding girders against corrosion requires careful consideration of the extent of damage, environmental conditions, and resource availability when selecting repair methods and materials [3]. Methods such as cleaning and re-protecting the corroded metal surface or

* Corresponding author: achmadzultan@gmail.com

http://dx.doi.org/10.28991/CEJ-2024-010-07-05

replacing sections or the entirety of the damaged girder can be utilized [4, 5]. Using materials that resist corrosion and possess robust structural integrity is crucial to guaranteeing the bridge's proper and safe operation once the repair process is finalized.

Corrosion in concrete structures poses a notable concern, potentially resulting in spalling, aesthetic deterioration, and a reduction in structural strength and longevity [6]. The primary culprit behind spalling is the corrosion of steel reinforcement, occurring when steel is exposed to moisture or humid conditions, initiating rust formation [7]. Salts and other substances transported by water have the potential to harm concrete structures by adhering to the surface of steel reinforcement and inducing corrosion. This corrosion leads to the development of cracks in the concrete cover layer, permitting the ingress of water and humid air, thereby intensifying the corrosion process [8]. The expansion of iron oxide or rust, which occupies more space than the original iron, results in an enlargement of the concrete volume. This generates harmful pressure as concrete exhibits low tensile strength [6]. Consequently, the corroded steel experiences erosion or corrosion, leading to a decrease in the cross-sectional area and overall strength of the structure [9]. Hence, it's crucial to conduct adequate maintenance to prevent and manage this issue of spalling. The ease of implementation and cost-effectiveness are key factors to consider when selecting repair techniques for addressing spalling damage on reinforced concrete structures [10].

This research seeks to thoroughly assess the efficiency of a hybrid repair approach utilizing both grouting and Glass Fiber-Reinforced Polymer (GFRP) through experimental trials. It explores the feasibility of applying this method in both controlled laboratory conditions and real-world settings. Previous studies have highlighted the promising efficacy of these repair materials. Cement grout, a specific type of grouting substance, has been shown to effectively fill voids, reinforce damaged concrete, improve temporary compressive strength, and reduce the risk of further deterioration [11–13]. Combinations of cement grout with various materials also significantly impact the restoration of flexural capacity [14], with GFRP combinations achieving up to 85% recovery of concrete's initial strength [15]. GFRP, as a reinforcing material, has demonstrated the ability to improve concrete's tensile and flexural strength in a composite manner, while also providing corrosion protection of up to 58% of its initial capacity [16, 17]. The combination of grouting and GFRP exhibits a synergistic effect that surpasses the strength of individual materials [18] and has proven beneficial for long-lasting reinforced concrete structures [19]. The importance of this research stems from its contribution to the progress of construction science and engineering. While concrete infrastructure typically lasts between 50 to 100 years on average, many structures have surpassed this age range, requiring suitable repair solutions to uphold their structural integrity over time. Conventional approaches frequently encounter challenges in sustainability, either due to exorbitant costs or recurring damage issues.

This research introduces a fresh approach by merging two promising materials: grouting and GFRP. Anticipated outcomes include thorough structural rehabilitation and complete functional recovery. Moreover, this method boasts advantages such as minimally invasive installation and competitive costs, in line with sustainable construction principles. The primary hurdle lies in realizing the widespread and sustainable adoption of this solution in practical applications. Comprehensive research, as outlined in this research, is essential to tackle this challenge. The insights gleaned from this research can offer guidance to engineers, researchers, and other stakeholders in crafting innovative, efficient, and eco-friendly repair solutions for more sustainable infrastructure in the future. By promoting sustainable construction practices, enhancing infrastructure longevity, and propelling the field of construction science and engineering, this research represents a significant stride towards a more sustainable, resilient, and environmentally friendly future for infrastructure.

## 2. Material and Methods

### 2.1. Material Characteristics

#### 2.1.1. Steel Reinforcement

Concrete beam samples were reinforced using three deformed bars, each with a diameter of 13 mm, and two plain bars, each with a diameter of 8 mm. Shear reinforcement comprised 8 mm diameter stirrups, spaced at intervals of 200 mm within the bending zone and 80 mm within the shear zone. The results from tensile strength tests, presented in Table 1 for both types of reinforcement, comply with the standards outlined in SNI 2052:2017. The plain reinforcement falls under the BjTP 280 category, while the 13 mm diameter deformed reinforcement falls under the BjTS 280 category. The modulus of elasticity employed in calculating the yield strain is 200,000 MPa. Tensile testing indicates that both types of reinforcement satisfy the criteria for use as reinforcement in reinforced concrete structures.

**Table 1. Characteristics of steel reinforcement**

| Bars | 8 (mm) | 13 (mm) |
|---|---|---|
| Diameter (mm) | 7.89 | 12.84 |
| Fy (MPa) | 376 | 316 |
| Fu (MPa) | 497 | 453 |
| Elongation (%) | 13 | 15 |

### 2.1.2. Concrete Mix Characteristics

In this research, fresh concrete with a maximum aggregate size of 20 mm, a sand content of 34.35%, and an aggregate content of 65.65% was employed. The slump test yielded a measurement of 12 cm, indicating that the concrete was easily workable. The compressive strength of the concrete was determined to be 21.82 MPa. The splitting tensile strength test, conducted following SNI 2491:2014 guidelines, utilized cylindrical specimens measuring 100 × 200 mm. The average splitting tensile strength of the three specimens was recorded at 1.90 MPa. For the flexural strength test of the concrete, beams with dimensions of 100 × 100 × 400 mm were utilized in accordance with SNI 4431:2011 standards. The average flexural strength, obtained from three specimens, was determined to be 4.06 MPa.

### 2.1.3. Grouting Mortar (Sikagrout-215)

Sikagrout-215 @25kg is a grout mixture made of cement, aggregates, and additives. It possesses qualities such as non-shrinkage, prevention of bleeding, and high strength. To assess its strength and properties, a sample of the grout measuring 50 x 100 mm and utilizing 25 kg of Sikagrout-215 material was subjected to testing. After 28 days, using a compression testing machine, the sample was evaluated. The results revealed an average compressive strength of 33.27 MPa, surpassing the typical strength of concrete at 21.82 MPa. This discrepancy indicates that grout has superior strength compared to regular concrete.

### 2.1.4. Glass Fiber Reinforced Polymer (GFRP) and Adhesive

The GFRP reinforcement utilized in the research originated from Fyfe Company, specifically Tyfo® - The Fiberwrap Composite System SEH-51A. Mechanical property testing of the GFRP was carried out according to ASTM D-3039, resulting in the creation of two specimens measuring 4 cm in width, 0.14 cm in thickness, and 20 cm in length. Tensile property testing of Fiber Reinforced Polymer (FRP) sheets was conducted using a Universal Testing Machine (UTM) with a capacity of 1000 KN, at a speed of 0.5 mm/sec. Epoxy adhesive emerged as a highly efficient method for adhering FRP to structural surfaces, offering several advantages over mechanical adhesives. These include the absence of stress concentration, ease of application, and preservation of the base or composite material. Detailed characteristics of the GFRP sheet and epoxy adhesive can be found in Tables 2 and 3, respectively.

**Table 2. State of GFRP composites**

| Material Properties | Test Score |
|---|---|
| Ultimate Tensile Stress | 575 MPa |
| Tensile Modulus | 26.1 GPa |
| Strain | 2,20% |
| Thickness of Composite | 1.3 mm |

**Table 3. Material characteristics of epoxy resin**

| Material Properties | ASTM Method | Test Score |
|---|---|---|
| Tensile Strength | ASTM D-638 | 72.4 MPa |
| Tensile Modulus | - | 3.18 GPa |
| Percent Strain | ASTM D-638 | 5% |
| Flexural Strength | ASTM D-790 | 123.4 MPa |
| Flexural Modulus | ASTM D-790 | 3.12 MPa |

## 2.2. Detail of Specimens

The research aimed to examine spalling damage on conventionally reinforced concrete beams replicated under field conditions at a 1:1 scale. The concrete beam measured 150 × 200 × 3300 mm and employed a 13 mm diameter deformed tensile reinforcement along with 8 mm stirrups. Figure 1 illustrates the initial state of the reinforced concrete beam before undergoing repair and reinforcement treatment, while Figure 2 portrays the beam's condition post-spalling damage, which led to a 52% reduction in tensile reinforcement. In response, the damaged area had its tensile reinforcement replaced with 8 mm diameter plain reinforcement. Repair of the spalling damage was conducted using Sikagrout-215@25 kg, a cement-based grouting material known for its non-shrinking properties. Additionally, reinforcement was implemented using GFRP sheets positioned at specific locations on the reinforced concrete beam. The research comprised four types of specimens, each yielding three samples. For further details, please consult Table 4.

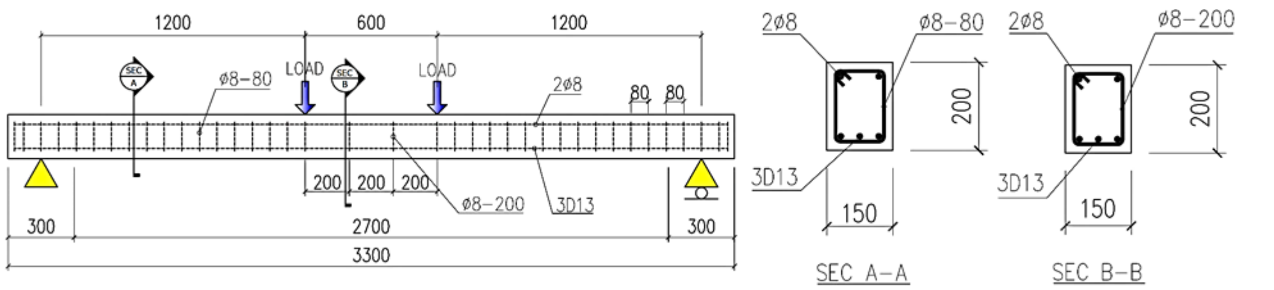


**Figure 1. Details and dimensions of control beams (BK) (Unit: mm)**

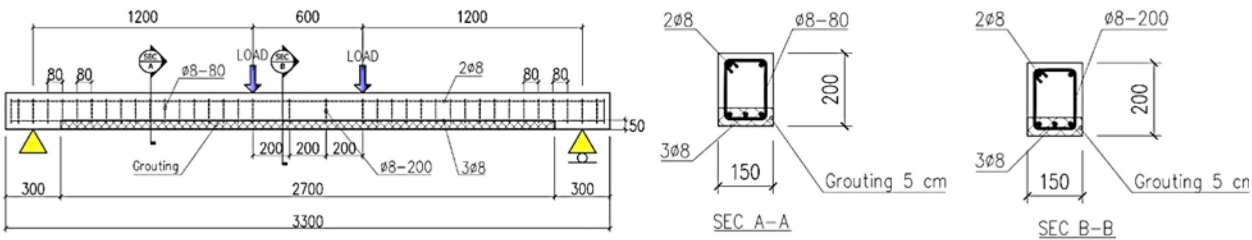


BGR variation type

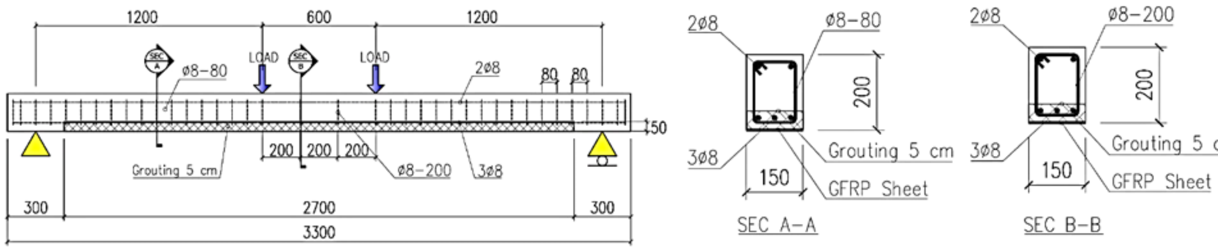


BGRS variation type

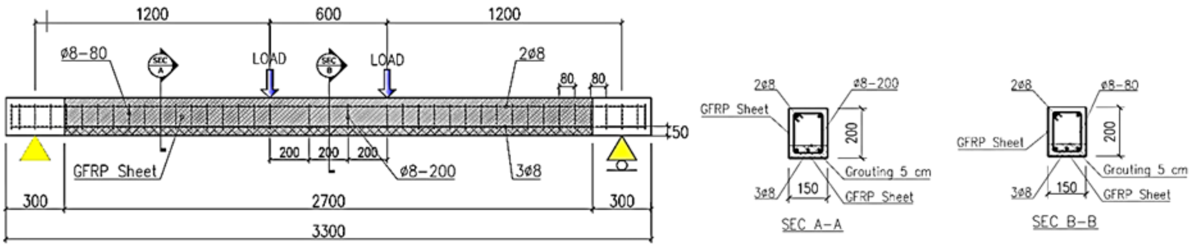


BGRSF variation type

**Figure 2. Details and dimensions of variation beams (Unit: mm)**

**Table 4. Details of test specimens**

| Beam code | Item | Action | Materials | Treatment of RC Beams |
|---|---|---|---|---|
| BK | 3 | Control | - | No |
| BGR | 3 | Grouting | Sikagrout-215. | 5 cm patch |
| BGRS | 3 | Grouting and reinforcement GFRP Sheet | Sikagrout-215, GFRP | 5 cm patch, GFRP strip on the bottom side |
| BGRST | 3 | Grouting, reinforcement GFRP Sheet, and full wrapping | Sikagrout-215, GFRP | 5 cm patch, GFRP strip on the bottom side, and full wrapping on the beam structure |

## 2.3. Fabrication Specimens

The specimen creation process comprised fabricating reinforced concrete (RC) beam specimens, grouting the RC beams, and incorporating Glass Fiber Reinforced Polymer (GFRP) as a reinforcement material. Initially, RC beam fabrication involved preparing and assembling steel reinforcement, pouring Sikagrout-215 mortar, preparing epoxy, and installing GFRP sheets. Notably, during the pouring stage, the concrete surface was not entirely covered, leaving a 5 cm border along a 3000 mm length. This indicates a possibility of delamination of the concrete cover surrounding the steel reinforcement within the reinforced concrete (RC) beam.

It was presumed that the variations in the bottom of the RC beam had experienced spalling to facilitate pouring and align with the research objectives. Consequently, the reinforced concrete beam was inverted to ease the pouring process and allow for the continuation of the work. The subsequent step involved grouting with Sikagrout-215 mortar combined with concrete that had undergone a curing period of 14 days. It is imperative to ensure that the aged concrete surface is devoid of any dirt or dust particles. Utilizing Sika adhesive as a bonding agent aids in establishing a seamless bond between the old and new concrete surfaces. Sikagrout-215 was employed to create a new joint, reinstating the dimensions of the RC beam and rectifying substantial damage resulting from the detachment of the concrete cover, which had penetrated to a depth of 5 cm. The RC beam specimen repaired using Sikagrout-215 was designated as BGR, and three RC beam specimens were readied for flexural testing.

The concluding phase entailed reinforcing the RC beam using GFRP composite. The process began by leveling the surface of the beam intended for GFRP layer reinforcement and thoroughly cleaning it to eliminate any dirt that might impede adhesion to concrete. Subsequently, components A and B of the epoxy resin adhesive mixture were prepared in a 2:1 weight ratio. Careful mixing was executed to prevent the formation of foam and bubbles, which could lead to the entrapment of air voids in the adhesive. The reinforcement material was then cut, and adhesive was applied lengthwise on the beam before being meticulously pressed onto the wet adhesive. To eliminate air voids between the reinforcement layer and the concrete surface, a roller was employed to press parallel to the reinforcement fibers. This ensured the adhesive bonded effectively to both the fibers and the concrete surface. A second layer of adhesive was applied across the entire surface of the Tyfo SEH-51 GFRP to enhance the robust adhesion of the fibers to the concrete surface. The key materials utilized in producing the specimens are depicted in Figure 3. Two variations in the installation of GFRP sheets on RC beams were implemented: reinforcement at the bottom position of the repaired RC beam (BGRS) and complete wrapping of GFRP around the RC beam (BGRSF). Figure 4 illustrates the procedural steps involved in creating RC beam specimens.

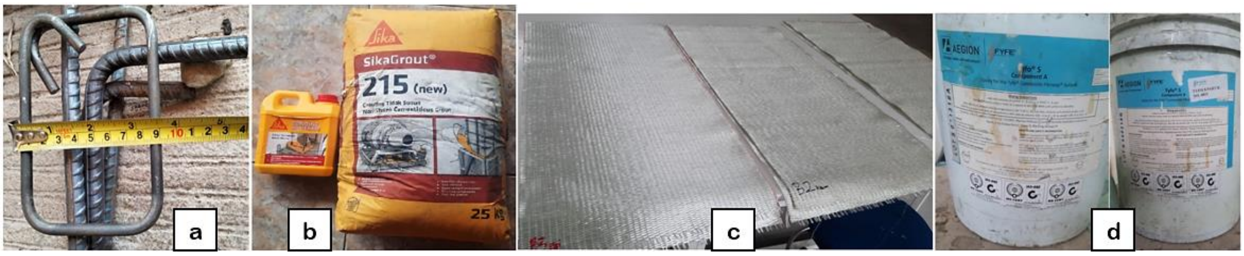


**Figure 3. (a) Iron reinforcement D 13 and ϕ8 (b) Sika cim bonding adhesive and Sikagrout-215 Mortar @25 kg (c) GFRP Woven sheet (d) epoxy resin FRP components A and B**


**Figure 4. (1) Casting of specimens assuming spalling age 0 days (2) 21 days old specimens ready for grouting (3) Production of Sikagrout-215 mortar @25kg (4) Patching post-spalling RC concrete with grouting mortar after coating with Sika cim bonding adhesive (5) Installation of GFRP sheets on RC beams after cleaning from all dirt (6) RC beam specimens ready for flexural strength test.**

## 2.4. The Testing Procedure for RC Beams

Reinforced concrete beams underwent flexural testing with four variations (BK, BGR, BGRS, and BGRSF) to evaluate their load-carrying capacity post grouting repair and reinforcement with GFRP composites (Figure 5). The testing employed a two-point bending test using a 100-ton flexural loading frame. Load measurement was facilitated by a load cell, while three LVDTs with a 100 mm range and 0.01 mm precision gauged deflection. Strain gauges monitored strain in steel, concrete, and GFRP. The testing apparatus consisted of a simple steel profile frame with pin-rollers, accommodating beams with a 3300 mm span and a square cross-section of 150 mm x 200 mm. Beams were supported with a clear span of 3000 mm, 1200 mm between loading points, and a shear span of 600 mm. Divided into three zones (as shown in Figure 1), Zones 1 and 3 experienced low bending moments but high shear loads, while Zone 2 faced high bending moments. To ensure precise deflection measurement, a load distribution beam atop the test beam evenly distributed the load. Figure 6 outlines the research methodology employed to achieve the research objectives.

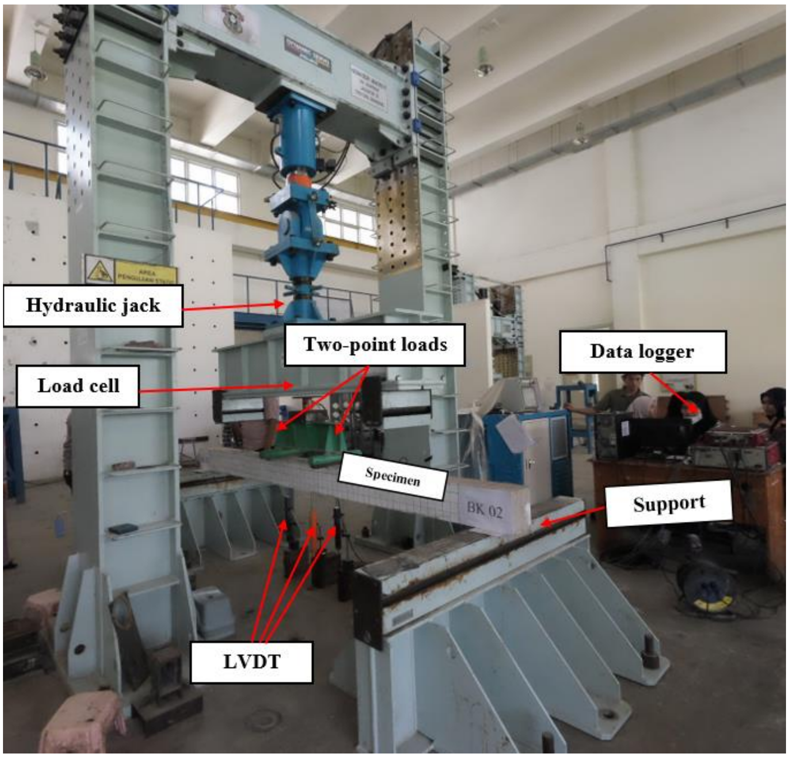


**Figure 5. Preparation for flexural strength testing using the UTM instrument**

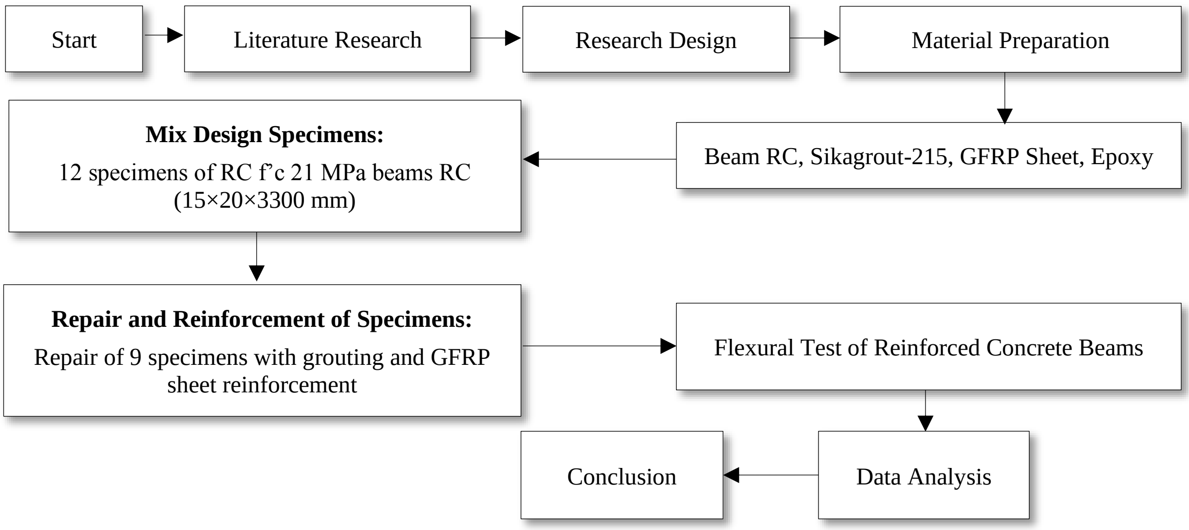


**Figure 6. Research procedure flowchart**

# 3. Results and Discussion

## 3.1. Load vs Deflection Behavior Relationship

Table 5 outlines the average results of testing conducted on reinforced concrete (RC) beams. Initially, the average load on three control beams at the onset of cracking was 2.61 kN, with a corresponding deflection of 1.29 mm at the midpoint of the beam. The first flexural crack appeared in zone 2 at the underside of the beam. As the load reached the yield point of 25.87 kN, the deflection increased to 17.67 mm. While the load increment was restrained in the subsequent loading phase, deflection continued to rise. At the peak load of 29.74 kN, the beam exhibited a deflection of 53.59 mm (Figure 7-a, Table 5). Three RC beams in a critical state, designated as BGR, underwent repair by applying grouting mortar to their lower surfaces. Upon reaching an average load of 2.38 kN on the BGR beam, a deflection of 2.18 mm occurred at the beam's midpoint. Steel reinforcement began yielding at an average load of 12.17 kN, corresponding to a deflection of 19.06 mm. Ultimately, the beam's load-bearing capacity was compromised, leading to collapse at a load of 14.39 kN with a deflection of 28.17 mm (Figure 7-b, Table 5). The BGR beam exhibited a notable 51.58% reduction in its load-bearing capacity compared to the control beam. This outcome contrasts with the research conducted by Ortega et al. (2018) [20], where the quality of the mortar led to an increase in load capacity of up to 65% compared to the control beam. It also contrasts with the research by [11, 18], where the grouting mortar successfully increased the load-bearing capacity by 72% and 120%, respectively.

**Table 5. Average value of RC beam test results**

| Beams | Concrete Cracking | | Steel Yielding | | Ultimate Stage | |
|---|---|---|---|---|---|---|
| | Load (kN) | Deflection (mm) | Load (kN) | Deflection (mm) | Load (kN) | Deflection (mm) |
| Control beam | 2.61 | 1.29 | 25.87 | 17.67 | 29.74 | 53.59 |
| BGR | 2.38 | 2.18 | 12.17 | 19.06 | 14.39 | 28.17 |
| BGRS | 7.22 | 4.85 | 20.35 | 24.97 | 27.81 | 50.24 |
| BGRSF | 7.24 | 2.96 | 21.54 | 21.60 | 32.14 | 47.72 |

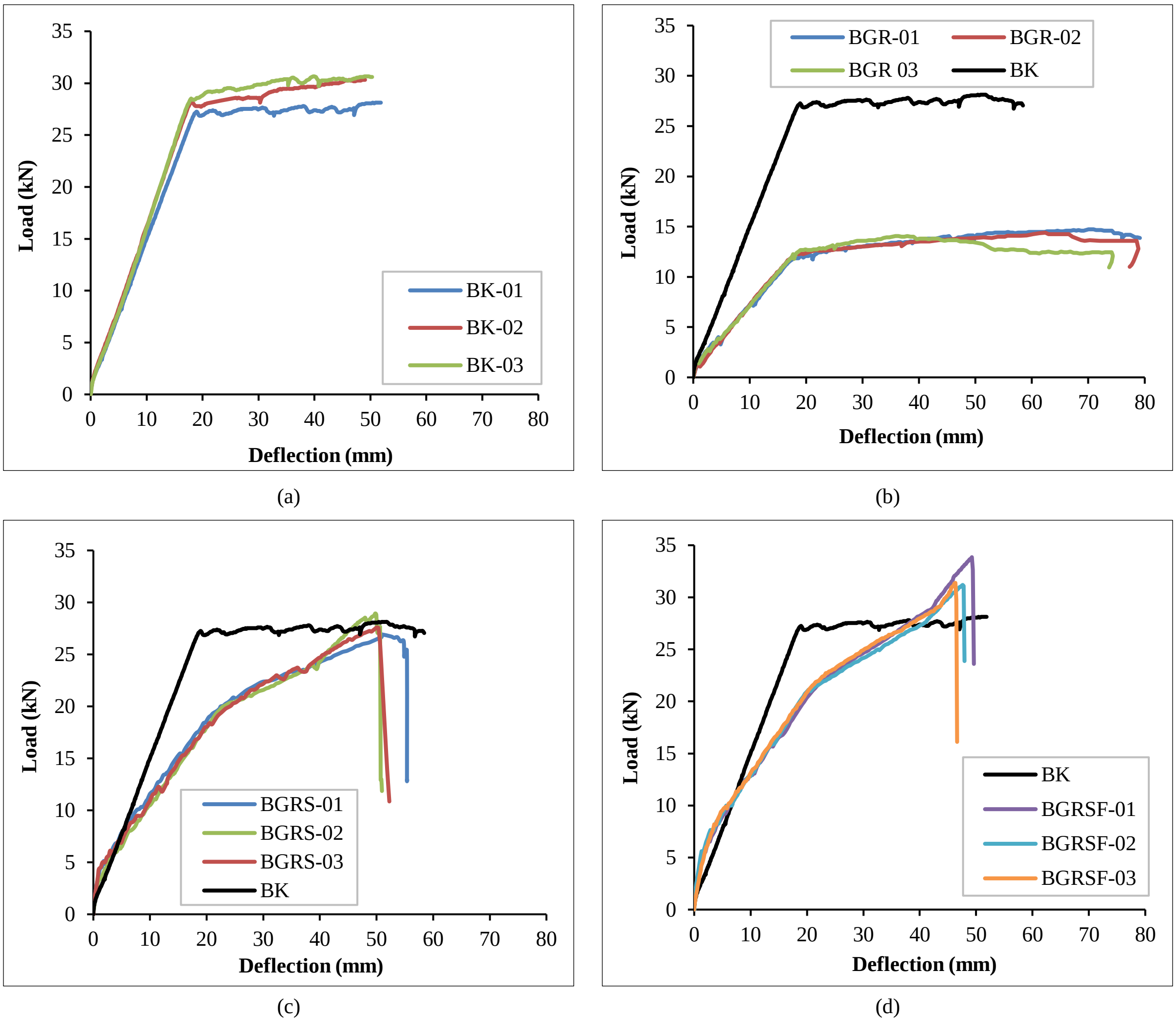


**Figure 7. Load and deflection relationship curves for specimens (a) BK, (b) BGR, (c) BGRS, and (d) BGRSF**

Hence, BGR-type beams necessitate more extensive repairs. For instance, incorporating additional materials such as GFRP sheets can offer enhanced mechanical reinforcement to the beam. Through these necessary repairs, it is anticipated that the beam will regain adequate load-bearing capacity to withstand loads and meet design requirements safely. One advantage of utilizing Sikagrout-215 mortar for repairs lies in its ability to effectively fill concrete gaps, thereby enhancing density. This process aids in reinstating the beam to its original dimensions and diminishes the likelihood of future damage. However, this repair approach is only appropriate when the beam's damage is not severe and its load-bearing capacity remains relatively high. If the beam's load-bearing capacity is already significantly compromised, repairing it with grouting mortar may prove ineffective, necessitating consideration of a more comprehensive repair method. Cracks in the grouting mortar on reinforced concrete (RC) indicate that the consistency between the old and new concrete impacts the concrete's quality. In such instances, the joint area can emerge as a weak point in the concrete structure, leading to cracks or damage. Continuous loading on the joint area, such as repeated or heavy static loads, can render it susceptible to cracking or damage.

Three reinforced concrete (RC) beams labeled as BGRS underwent rehabilitation using Sikagrout-215 mortar and reinforcement with a composite GFRP sheet on the bottom surface. At an average load of 7.22 kN, a deflection of 4.85 mm was observed at the midpoint of the beam, with the first flexural crack appearing at the bottom of the second zone of the beam. As the load reached 18.50 kN, reinforcement began to yield, and the deflection at this load was approximately 24.97 mm. Upon reaching a load of 27.81 kN, the beam exhibited a deflection of 50.24 mm, leading to loss of its bearing capacity and eventual collapse (Figure 7-c - Table 5). The reinforcement of BGRS RC beams with grouting and composite GFRP sheets resulted in a 6.49% decrease in ultimate load-bearing capacity compared to the control beam. Previous studies [19, 21] have effectively reinforced the bottom surface of the beam, preserving the structural integrity of the beam under repeated loads and extreme conditions.

Employing a composite GFRP sheet on the underside of the concrete (BGRS) has not entirely reinstated the beam's original functionality akin to the control beam. Nonetheless, it can extend the service life under load compared to complete concrete replacement. The reduction in the ultimate load-bearing capacity of BGRS is ascribed to the substandard quality of the reinforced concrete material and the inferior quality of reinforcement in the test specimen relative to the control beam [22]. The reinforcement procedure might not consistently yield optimal outcomes, leading to less-than-ideal enhancements in maximum load-bearing capacity. Nonetheless, if the attained load value aligns with the prerequisites for structural safety and reliability, the repair can be deemed successful in fortifying damaged or vulnerable structures [23].

Three RC beams labeled as BGRSF underwent reinforcement via grouting and complete wrapping along the entirety of the beam structure. Upon reaching an average load of 7.24 kN on the BGRSF beam, a deflection of 2.96 mm was recorded at the midpoint, with the first flexural crack emerging in the second lower zone. When the load reached 21.54 kN, the reinforcement began yielding, resulting in a deflection of approximately 21.60 mm. Ultimately, at a maximum load of 32.14 kN, the beam exhibited a deflection of 47.72 mm, leading to loss of its bearing capacity and eventual collapse (Figure 7-d and Table 5). The utilization of GFRP on the BGRSF beam structure demonstrated a significant impact. The reinforcement on beams in critical condition was able to increase the load capacity of the control beam by 8.1% [24, 25]. In a research employing diverse reinforcement configurations utilizing GFRP akin to the BGRS model, enhancements in strength of 118% and 90% were attained in comparison to the control beam [26, 27].

Even though the RC concrete beam collapsed, the comprehensive GFRP reinforcement notably augmented the beam's capacity, enabling it to endure a higher load before reaching the failure threshold. Implementing full GFRP reinforcement on the beam substantially bolsters structural rigidity by establishing a sturdy mechanical connection between GFRP and concrete, thereby facilitating effective force transmission and enhancing overall beam stiffness [28]. An even distribution of load along the beam is another advantage of full GFRP reinforcement, which reduces load concentration at critical points [29] and helps prevent failure or cracking in the beam. The stiffness imparted by GFRP reinforcement allows the beam to undergo both elastic and elastoplastic deformation without experiencing notable cracking [28].

## 3.2. Comparison of Load and Strain Behavior of Concrete Reinforcement

The strain of the steel reinforcement in the test specimen was monitored utilizing a strain gauge of type FLAK-2-11-5LJC-F with a gauge factor of 2.09±1%. Strain data was captured using a TDS 530 logger and subsequently transferred to computer software for further analysis. Recording took place whenever there was a variation in load induced by the hydraulic pump. The hydraulic pump applied a load, which was registered by the load cell and utilized to gauge the strain of the steel reinforcement. Based on the mechanical characteristics testing of steel reinforcement, a yield strain ($\varepsilon y$) of 1589 με was determined for D13 reinforcement and 1879 με for ϕ8 reinforcement.

Figure 8-a illustrates that the BK beam encountered steel reinforcement yielding at an average load of 25.87 kN, with a steel strain of 1771 $\mu\varepsilon$. In the research, it was found that the BK beam experienced failure at a load of 29.74 kN, accompanied by a steel strain of 3620 με. The relationship between load and strain in the BK beam is initially linear until reaching the yield point. Beyond this point, the relationship becomes nonlinear, indicating the onset of plastic deformation, leading to a loss in load-bearing capacity. Araby et al. (2022) [30] noted that beams reinforced with threaded steel exhibit a lower yield strain compared to independently tested steel reinforcement. Similarly, Kioumarsi et al. (2021) observed plastic deformation occurring post-yield point in beams reinforced with threaded steel.

In Figure 8-b, BGR 01, BGR 02, and BGR 03 underwent steel reinforcement melting once they reached their respective yield loads. Specifically, BGR 01 melted at a yield strain of 1989 με and a yield load of 11.99 kN, BGR 02 melted at a yield strain of 2123 με and a yield load of 12.60 kN, and BGR 03 melted at a yield strain of 2191 με and a yield load of 11.93 kN. Subsequently, all three beams failed at their respective ultimate loads: 14.73 kN with an ultimate strain of 2114 με for BGR 01, 14.39 kN with an ultimate strain of 2256 με for BGR 02, and 14.06 kN with an ultimate strain of 2434 με for BGR 03. Additionally, this research included separate mechanical testing of steel reinforcement. A yield strain of 1879 με was found for steel with a diameter of φ8. A comparison with the average yield strain of the BGR beams reveals that the yield strain of the BGR beams is higher than that of the steel reinforcement tested independently.

Figure 8-c depicts the deformation experienced by beams BGRS 01, BGRS 02, and BGRS 03 in the melted steel reinforcement, with an average yield strain of 2416 με and an average yield load of 19.18 kN. Beam BGRS 01 experienced structural failure when subjected to an ultimate load of 26.92 kN, while beams BGRS 02 and BGRS 03 failed at 28.92 kN and 27.59 kN, respectively. In the mechanical testing of ϕ8 steel reinforcement, a yield strain of 1879 με was identified. However, the yield strain of the steel reinforcement in the BGRS beam significantly surpassed this value. This deviation can be attributed to the reinforcement of GFRS on the compression side of the BGRS beam, which enhances the bending structure's stiffness. This increased bending stiffness enables the steel reinforcement to endure tensile stresses resulting from larger bending moments without yielding. Consequently, the BGRS beam exhibited higher yield strain characteristics and a more extensive plastic phase compared to the BK beam. In the BGRS beam, the yield strain ranged from 2249 με to 2641 με, while in the BK beam, it ranged from 1624 με to 2008 με. The robust tensile characteristics of GFRP allow it to absorb a portion of the tensile stresses produced by bending within the beam [8, 31, 32]. Consequently, some of the bending strain previously carried by the steel reinforcement is shifted to GFRP. In this scenario, employing GFRP to withstand bending tensile stresses results in a reduction of the strain experienced by the steel reinforcement [33]. When compared to the BK beam, it is evident that the installation of GFRP on the tension side of the BGRS beam significantly decreases bending strain in the steel reinforcement.

In Figure 8-d, beam BGRSF 01 exhibited steel reinforcement yielding at a yield strain of 1567 με with a yield load of 21.25 kN, ultimately failing at a load of 33.85 kN. Beam BGRSF 02 similarly experienced steel yielding at a yield strain of 1748 με with a yield load of 21.46 kN, failing at an ultimate load of 31.19 kN. Beam BGRSF 03 underwent steel yielding at a yield strain of 2075 με with a yield load of 21.92 kN, ultimately failing at a load of 31.39 kN. The yield strain of steel reinforcement in the BGRSF beam is 1.4% lower than that of the BK beam. However, the yield load of the BGRSF beam is 16.71% lower, while the ultimate load is 8.08% higher than that of the BK beam. Excessive utilization of GFRP may potentially lead to a reduction in the bending stiffness of the beam and weaken the bond between the steel reinforcement and concrete [18, 23]. The test results indicate that the average yield strain of steel in the BGRSF beam, reinforced with GFRS, is 1797 με, representing a reduction of approximately 4.4% compared to the yield strain of steel reinforcement achieved through mechanical methods. The BGRSF beam demonstrates superior resistance to steel deformation compared to the BGR and BGRS beams.

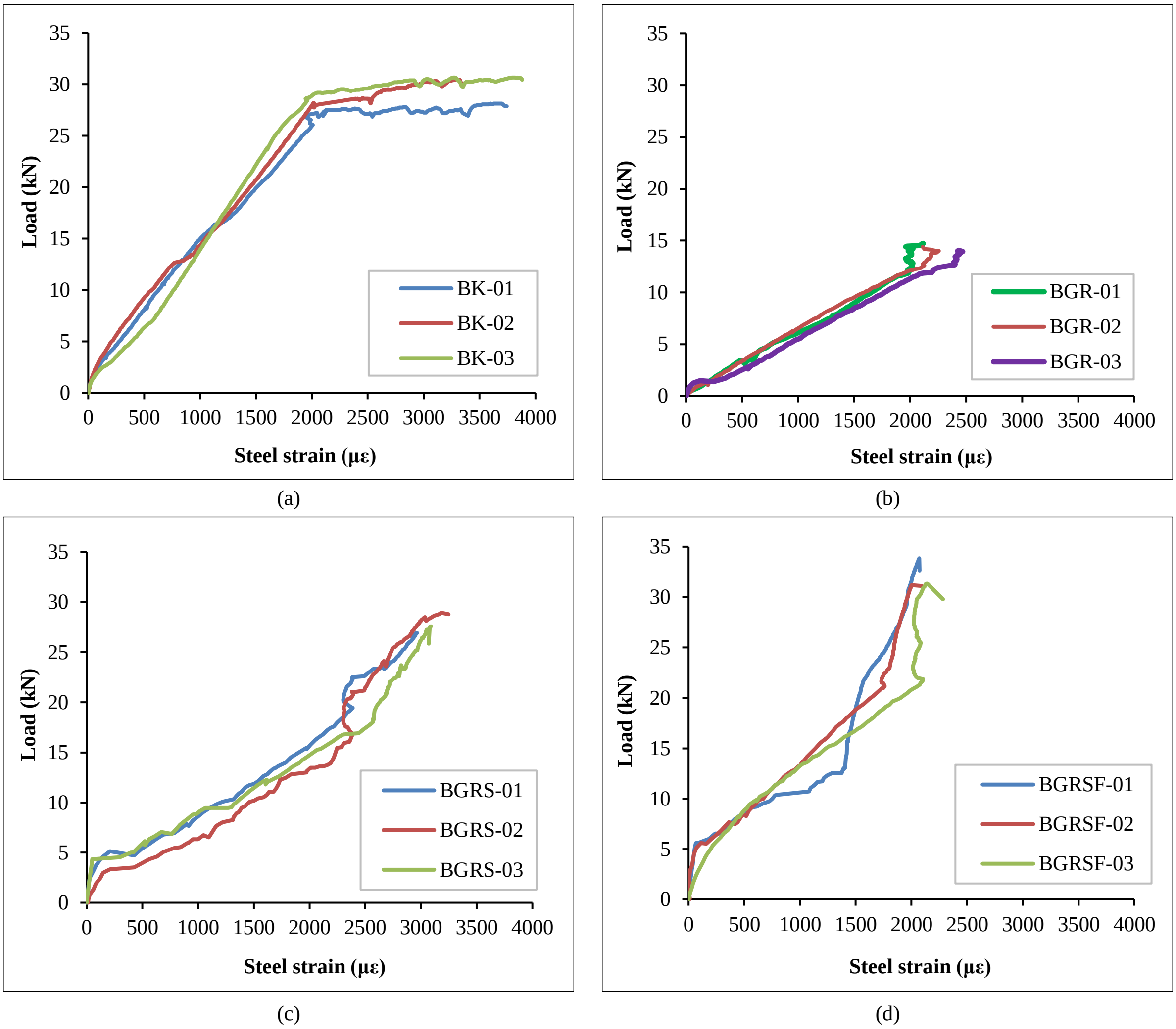


**Figure 8. Load-strain curves of steel in beams: (a) BK, (b) BGR, (c) BGRS, (d) BGRSF**

### 3.3. Comparison of Load and Strain Behavior of Concrete

In this research, concrete strain was assessed employing a PL-60-11-5L strain gauge, characterized by a gauge factor of 2.09±1%. The TDS 530 data logger was employed to gauge the concrete strain increase with a precision of 0.001%. Subsequently, the data logger was connected to computer software for analysis. Concrete strain data was logged for each variation in load induced by the hydraulic pump, with this data captured by the load cell and transmitted to the test specimen. Consequently, the concrete strain data could be associated with load data to construct a concrete stress-strain diagram.

In Figure 9-a, the conventional reinforced concrete beam (BK) showcases impressive bending characteristics. With an average yield load of around 25.87 kN and a yield strain of 1159 με, it suggests that the beam can sustain the load until the steel reinforcement reaches its yield point without experiencing notable permanent plastic deformation. The concrete in the control beam (BK) displays performance that surpasses expectations. The average concrete strain recorded for BK upon reaching the maximum load, namely 2811 με, has surpassed the anticipated ultimate strain value of 3000 με. This indicates that the concrete in the control beam exhibits greater resistance to deformation than initially expected. Overall, the standard BK beam displays exceptional bending performance, capable of withstanding substantial loads until reaching the ultimate condition, where it may incur significant structural damage. This aligns with the anticipated flexural performance of typical reinforced concrete beams. Naser et al. (2019) [34] demonstrated that increasing the diameter of the steel reinforcement can enhance the beam's strength and stiffness. Al-Asadi et al. (2019) [31] noted that the utilization of such additives can augment the strength and deformation resistance of reinforced concrete beams.

The analysis outcomes depicted in Figure 9-b reveal a decrease in the load capacity of the BGR beam subsequent to its damage and subsequent repair with grouting. Both the average yield load and ultimate load values of the BGR beam are inferior to those of the undamaged BK beam. Moreover, the yield strain and ultimate strain of the BGR beam also exhibit lower values, indicating a decline in the beam's bending stiffness following grouting repair. The effectiveness of grouting repair on the BGR beam in restoring its bending capacity appears to be limited. Hence, additional repairs utilizing alternative methods, such as GFRP reinforcement, are necessary to reinstate the beam to its original strength prior to damage. Nevertheless, the ultimate strain of the BGR beam still surpasses the ultimate strain value of the concrete before failure, suggesting that the BGR beam demonstrates greater resilience to strain than the pre-failure condition. This research contrasts with the research conducted by Djamaluddin et al. (2015) [32], which illustrated that grouting can rejuvenate the bending strength of corroded reinforced concrete beams affected by reinforcement corrosion. Chen et al. (2021) [13] observed that employing suitable grouting material can bolster strength, stiffness, and diminish cracking and deformation in beams afflicted by structural fatigue.

The analysis depicted in Figure 9-c demonstrates a reduction in the maximum load capacity of the BGRS beam, as evidenced by the average ultimate load (Pu) and yield load (Py) values of 27.81 kN and 18.50 kN, respectively. Furthermore, there is a decline in the bending stiffness of the beam, indicated by the yield strain ($\mathcal{E}c$ yield) value of 753 με and ultimate strain ($\mathcal{E}c_{\text{ulti}}$) value of 1877 με in the BGRS beam. These outcomes suggest that the combination of grouting and GFRP reinforcement has not completely reinstated the strength and stiffness of the BGRS beam to its original state, as observed in the BK control beam. Although the ultimate strain of the BGRS beam remains below the ultimate strain value of normal concrete, set at 3000 με, the improvement in post-spalling flexural performance of the beam has been suboptimal. The integration of grouting repair methods and the incorporation of GFRP has not entirely restored the bending capacity of the BGRS beam following spalling. This could be attributed to insufficient adhesive bond strength or the presence of leaks, which might hinder the grouting from adequately filling gaps or effectively restoring the bending strength of the beam. Consequently, careful selection and proper installation of GFRP reinforcement are imperative to withstand significant structural loads [12]. Insufficient strength or inadequate planning of GFRP reinforcement may limit its ability to enhance stiffness and enhance the bending capacity of the beam. Therefore, it is crucial to develop more appropriate methods to fully restore the bending performance of the BGRS beam to its original condition before spalling damage occurs.

The test results depicted in Figure 9-d indicate that the average yield load (Py) value for the BGRSF beam is 21.54 kN, accompanied by a yield strain (Ɛc yield) of 1048 με. Moreover, the average ultimate load (Pu) value for the BGRSF beam is 32.14 kN, with an ultimate strain (εc ulti) of 2525 με. Compared to the control beam BK, the ultimate load of the BGRSF beam increased by 8.05%. The decrease in yield strain in the BGRSF beam, as opposed to BK, is attributed to the presence of GFRP reinforcement, which limits beam deformation under load. GFRP aids in restraining beam strain to prevent it from exceeding acceptable limits during the elastic stage. Consequently, the yield strain value of the BGRSF beam is lower than that of BK, BGR, and BGRS. The heightened ultimate load observed in the BGRSF beam compared to BK underscores the enhanced strength and bending stiffness resulting from GFRP reinforcement. GFRP helps increase the tensile strength of the beam by uniformly distributing the load along the reinforcement [22, 24, 33] stated that the installation of GFRP on the sides of the beam helps to resist tensile forces caused by bending, enabling the beam to withstand a larger ultimate load before failure compared to

BK, BGR, and BGRS. The BGR beam displayed the highest proportion of concrete strain at 93.3%, with the BGRSF beam following at 84.8% and the BGRS beam at 66.7%. This suggests that the BGR beam offers superior resistance to concrete deformation compared to the other beams.

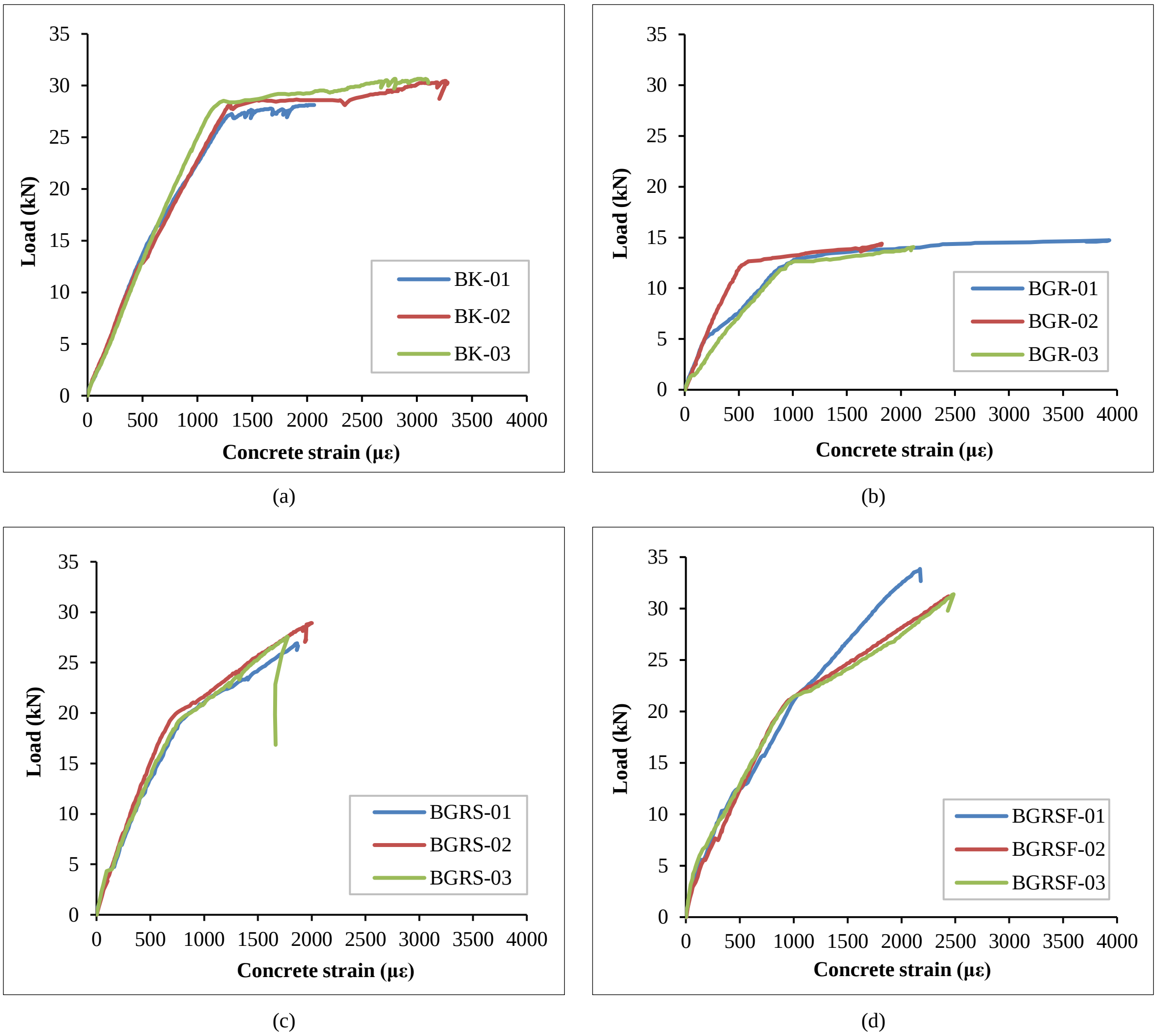


**Figure 9. Load-strain curves of concrete in beams: (a) BK, (b) BGR, (c) BGRS, (d) BGRSF**

### 3.4. Comparison of Load and Strain Behavior of GFRP

In this research, GFRP strain was measured using a FLAB-2-11-5LJC-F strain gauge installed on the GFRP material to track strain occurrences. The strain gauge recorded the strain data, which was then transmitted in real-time to a computer via the TDS 530 data logger. This data logger has the capability to record strain data at a rate of up to 1000 data points per second. GFRP strain is defined as the ratio of the change in length to the initial length of the GFRP material. As the load applied to the reinforced concrete beam increases, the strain in GFRP also increases. The rate of increase in GFRP strain is directly proportional to the applied load. GFRP strain reaches its maximum value when the beam reaches its maximum load, indicating that GFRP strain increases as the load on the beam increases.

Figure 10-a depicts that in the BGRS01 specimen, the GFRP strain at the ultimate load (Pu) of 26.92 kN is 8149 με. In BGRS02, the GFRP strain reaches 11616 microstrains at the ultimate load (Pu) of 28.92 kilonewtons. Meanwhile, in BGRS03, the specimen shows a GFRP strain of 10032 με at the maximum load (Pu) of 27.59 kN. The higher GFRP strain in BGRS02 compared to BGRS01 and BGRS03 suggests that BGRS02 can withstand a larger load. As the bending load on the concrete beam increases, the tensile stress on the bottom of the beam also rises. Since GFRP is designed to withstand tensile stress, the greater the bending load, the higher the GFRP strain. However, the maximum GFRP strain of 22,000 με (as shown in Table 2) far exceeds the recorded GFRP strain. This suggests that the GFRP did not rupture at the ultimate load but may have experienced debonding before reaching its strain capacity.

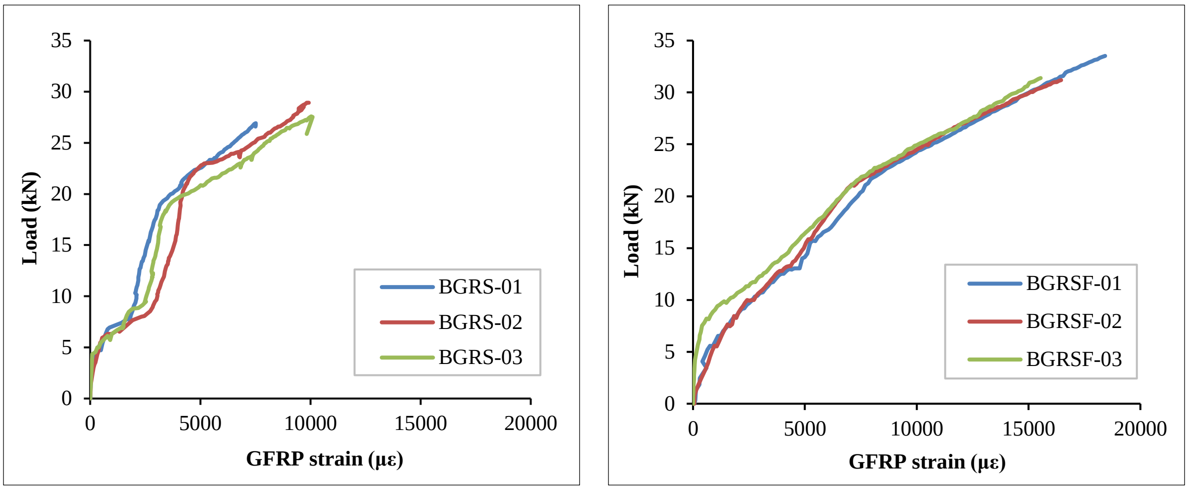


(a) (b)

**Figure 10. Load-strain curves of GFRP in beams: (a) BGRS, (b) BGRSF**

Figure 10-b indicates that the three BGRSF specimens recorded GFRP strain values ranging from 14,000 to 18,000 με upon reaching maximum and ultimate loads. BGRSF01 displays a GFRP strain of 18424 με at the ultimate load (Pu) of 33.85 kN. In BGRSF02, the GFRP strain measures 16456 microstrains at the ultimate load (Pu) of 31.19 kilonewtons. Meanwhile, in BGRSF03, the specimen exhibits a GFRP strain of 15541 με at the maximum load (Pu) of 31.39 kN. Among the three types of beams, the BGRSF beam records the highest GFRP strain, measuring 18424με. Comparatively, the BGRS beam has an average GFRP strain of 9933 με, while the BGRST beam has an average GFRP strain of 14256 με. This suggests that the BGRSF beam is more flexible and capable of enduring more deformation before failure occurs. The GFRP reinforcement method employed on the BGRSF beam is brittle and cannot undergo plastic deformation like steel. Consequently, reinforced concrete beams with GFRP tend to be less ductile and more brittle [23]. Upon reaching its load capacity, the GFRP beam experiences sudden failure without any preceding deformation, unlike a conventional reinforced concrete beam. Additionally, an excessive installation of GFRP can render the beam excessively stiff when subjected to bending, potentially causing it to fail in shear before reaching its bending capacity [35, 36]. As the quantity of GFRP utilized increases, the strain in GFRP escalates progressively from the BGRS beam (9933 με) and BGRST beam (14256 με) to its peak in BGRSF (16807 με). This augmentation in GFRP strain is directly correlated with the beam's improved capacity to endure bending loads by shifting stress from concrete to GFRP.

## 3.5. Crack Pattern in Reinforced Concrete Beams

The cracks observed in the five types of beams were predominantly flexural cracks, characterized by a vertical crack pattern originating from the tensile side and extending upward towards the neutral axis. These flexural cracks resulted from the beams' inability to withstand loads surpassing their strength. Typically, the initial crack emerged in the middle third of the span under the load and propagated extensively from the tensile side towards the compressive side. The crack continued to propagate until reaching the peak load, coinciding with the maximum load reached and an increase in deflection. As the crack widened towards the neutral axis, it then underwent a significant reduction, diminishing the stiffness of the beam.

The failure exhibited ductility, with the tensile reinforcement yielding initially. GFRP-reinforced beams demonstrated the ability to endure higher loads before crack initiation and propagation compared to conventional beams [17, 37]. This illustrates GFRP's efficacy in augmenting the load capacity of concrete beams before failure. In general, the observed flexural crack patterns in the five types of beams were in line with the theory of reinforced concrete beam behavior under flexural loads. GFRP has been shown to improve crack resistance and load capacity before ductile failure ensues [22]. At their maximum load, the beams managed to endure it despite the considerable widening of cracks. Nonetheless, the deflection of the beams was already notably pronounced in these circumstances. Subsequent to reaching the maximum load, the beams still maintained support, albeit with a decreasing load. However, the deflection of the beams continued to rise significantly [25]. The persistent deflection signifies a decrease in the beams' stiffness due to the widening cracks. These flexural cracks will persist in propagating from the tensile side to the compressive side of the beam until the beam eventually collapses. The failure is indicated by the beam cross-section damage resulting from the widening cracks. The observed flexural crack patterns on the beam specimens suggest that the beams failed due to flexural loads surpassing their capacity, evident in significant deflections leading to beam destruction. The crack patterns for each specimen are illustrated in Figures 11 to 14.

In Figure 11-a, observations reveal that the initial crack emerged when the load reached 3.4 kN, indicating significant elastic deformation within the beam's material structure. Subsequently, the yielding process ensued when the load reached 26.18 kN, signaling that the material had reached its endurance limit. The ultimate failure occurred under a maximum load of 28.12 kN, at which point the BK beam could no longer endure the applied bending stress, leading to failure. The length of the cracks formed had surpassed 3/4 of the beam span, indicating a substantial bending failure. A total of 25 crack patterns formed upon reaching the maximum load. Crack patterns emerging during bending failure tend to align with the direction of the bending stresses in the beam. This suggests that cracks are more likely to propagate parallel to the direction of the applied load, following the bending line on the beam. These cracks may become more concentrated and longer as the load increases until reaching maximum failure.

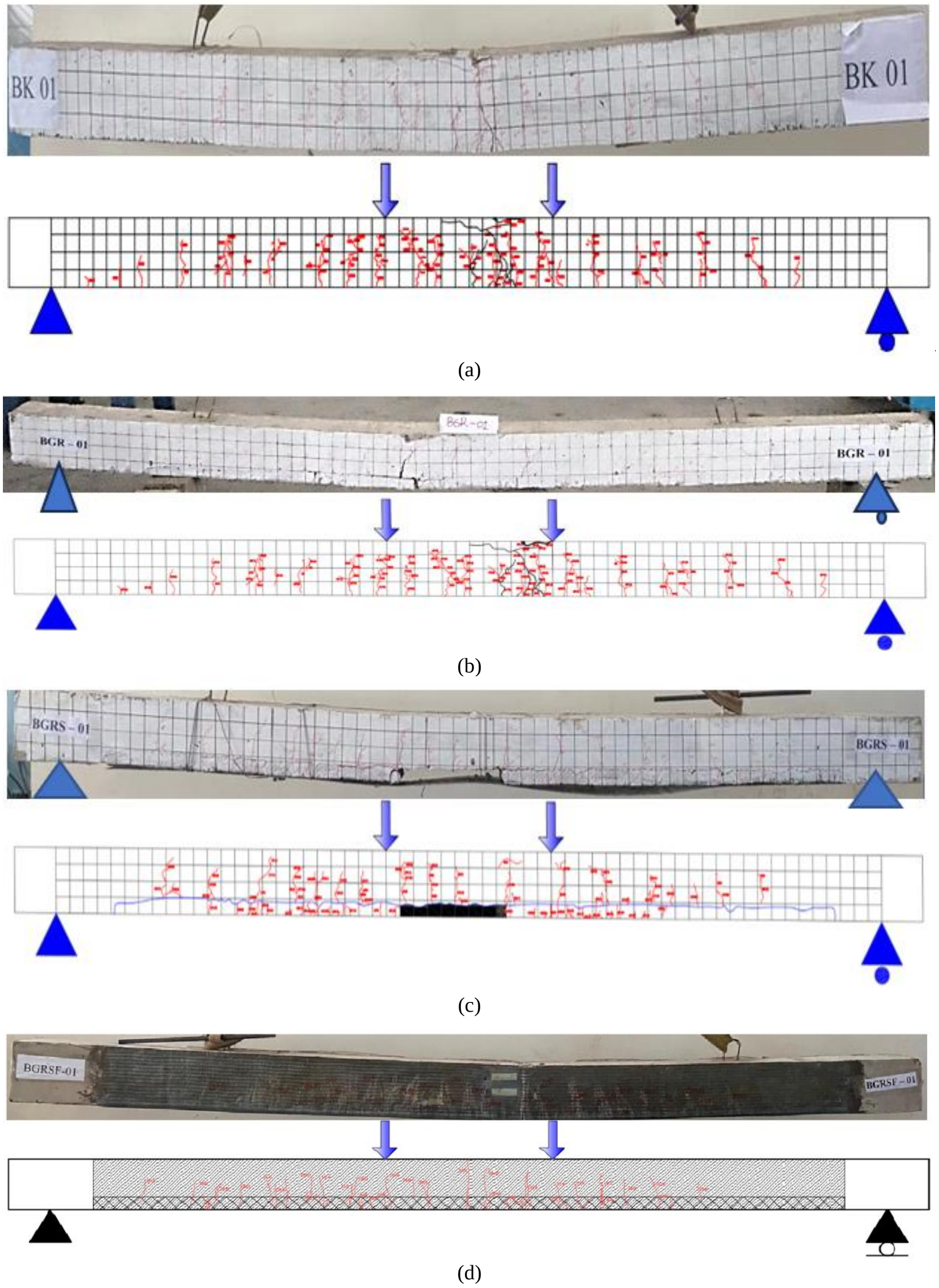


**Figure 11. Crack patterns in RC beams: (a) BK, (b) BGR, (c) BGRS, (d) BGRSF**

In Figure 11-b, the BGR specimen illustrates that upon reaching the beam's bending capacity, the first flexural crack emerged at 3.47 kN on the bottom side of the beam in the region of maximum bending moment, approximately 1/3 of the span. As the load intensified, the initial flexural crack continued to elongate and widen from the tensile side to the compressive side of the beam. At 11.99 kN, the beam's tensile reinforcement began to yield, indicated by permanent deformation. The maximum load of 14.73 kN was attained when the flexural crack had extended beyond the beam's neutral axis, approximately 3/4 of the span. Vertically, flexural cracks initiated on the bottom side of the beam in the region of maximum bending moment, progressing upwards towards the beam's neutral axis while branching out. Approximately 18 branching flexural crack grooves were observed. Horizontally, cracks emerged along the interface between the old concrete and the grouted concrete, spanning from one end of the interface to the other. Horizontal cracks on the interface plane of the two concrete layers indicate early delamination between the concretes due to imperfect bonding (poor adhesion). Following the maximum load, the beam underwent ductile failure, characterized by excessive deflection and destruction of the beam cross-section.

Figure 11-c depicts that under the initial condition without load, the BGRS beam, which underwent grouting due to spalling, remained intact without any cracks. As loading commenced, at a load of 7.86 kN, the first flexural crack emerged on the bottom side of the beam in the region of maximum bending moment. The flexural crack continued to propagate vertically and extended towards the center of the beam span, with approximately 21 vertical crack patterns observed. The number is higher than that of the BGR beam because the addition of GFRP reinforcement augments the beam's stiffness, resulting in more closely spaced cracks. Despite the increased number of crack patterns, the BGRS beam was able to achieve a maximum load of 26.92 kN, approximately 15% greater than that of the BGR beam. This illustrates that GFRP effectively functions as external flexural reinforcement, enhancing the maximum load capacity of reinforced concrete beams. During crack propagation, some small cracks may coalesce to form a single dominant crack. In addition to vertical cracks, horizontal cracks are also evident at the interface between the old concrete and the grouted concrete, indicating a weak bond between the two concrete surfaces. Subsequently, the specimen underwent yielding at a load of 19.79 kN until finally reaching a maximum load of 26.92 kN. At the maximum load, accompanied by a loud sound, the GFRP detached entirely from the surface of the beam. This failure arises as the GFRP endeavors to bear the load instead of the melted steel reinforcement. The vertical crack has extended beyond the beam's neutral axis, and the horizontal crack is notably wide. In this scenario, the BGRS beam underwent structural failure, marked by the complete destruction and detachment of the entire GFRP from the surface of the beam.

Upon observing the crack pattern of the BGRSF beam in Figure 11-d, it's apparent that the initial flexural crack emerged on the bottom side of the beam in the region of maximum bending moment when the load reached 5.53 kN. With increasing load, a single flexural crack propagated vertically from the tensile region to the compressive region, extending beyond the neutral axis of the beam cross-section. Additionally, several inclined cracks began to form at both ends of the GFRP strip due to the concentration of shear stresses in that area. At a load of 21.25 kN, the primary tensile reinforcement of the beam underwent yielding, evidenced by plastic deformation. Upon reaching the maximum load of 33.85 kN, the flexural crack had extended beyond 3/4 of the beam span. When the maximum load was attained, the tensile stress in the GFRP layer surpassed the interface bond strength between GFRP and concrete, resulting in a shear crack pattern characterized by vertical white streaks extending from the tensile to the compressive region of the beam. A total of 20 crack patterns were observed on the GFRP, indicating that the cracks had spread almost across the entire beam cross-section. Ultimately, the beam experienced flexural failure after the entire layer of GFRP cracked. Overall, the failure pattern of the BGRSF beam was characterized by crack streaks along the span and did not involve debonding of the GFRP layer.

### 3.6. Failure Mode of Beams with GFRP Reinforcement

Upon observing the failure mode of the BGRS beam in Figure 12, it's apparent that delamination and FRP failure have transpired in the form of detachment of the bond between the GFRP and the concrete surface (debonding failure). The delamination process initiates with the development of microcracks between the existing concrete and the grouted concrete in the central span, where the highest bending moment is experienced. Due to excessive tensile stress, these cracks propagate, resulting in the detachment of the new joint, which is 5 cm thick. The delamination crack at the interface between the existing concrete and the grouted concrete hinders the flexural crack in the grouting mortar from extending into the existing concrete. Furthermore, transverse cracks also form along the beam at the interface, indicating debonding of the GFRP strip. The loss of GFRP strength resulting from detachment from the concrete surface leads to a reduction in the bending capacity of the beam. The failure between the GFRP and the concrete occurs after the beam reaches a load of 28.92 kN, at which point the strain in the GFRP has reached 11616 με, surpassing the material's ultimate limit. Hence, delamination and debonding of GFRP represent critical failure modes in BGRS beams.. Research [19, 25] indicates that delamination commonly occurs as a failure mode in reinforced concrete beams reinforced with GFRP using the grouting method.

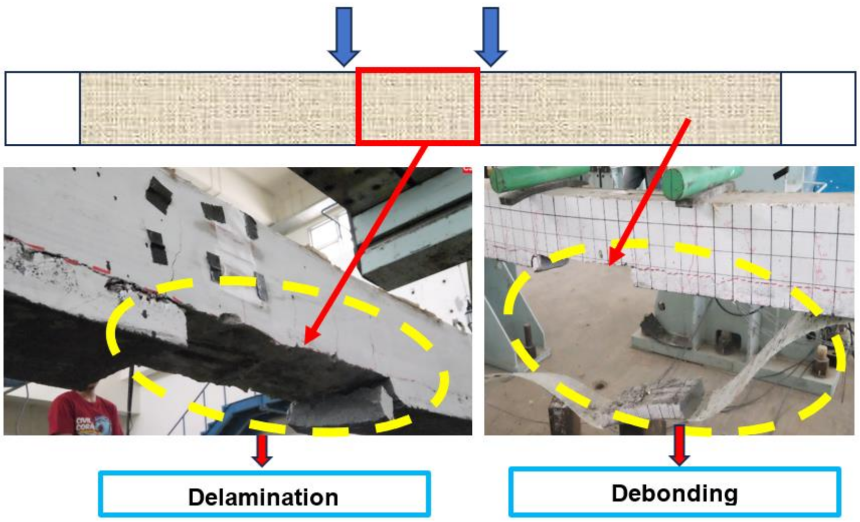


**Figure 12. Failure mode of Concrete Beam BGRS**

Based on the observations in Figure 13, it can be deduced that the initial flexural crack in the BGRS beam originated in the 1/3 span area, known as the zone of maximum bending moment, at a load of 6.73 kN due to tensile stress surpassing the concrete's tensile strength. With increasing load, a single flexural crack extended vertically from the tensile region to the compressive region of the beam, forming a flexural crack pattern. When the load reached 26.8 kN, the maximum crack width had reached 1.6 mm, indicating that the beam had exceeded its yield capacity. This maximum crack width of 1.6 mm already surpasses the typical serviceability limit for reinforced concrete structures, which is usually around 0.3 mm. Consequently, this suggests that the beam is already in an ultimate condition. Therefore, the subsequent debonding of GFRP emerges as the primary cause of flexural failure in the BGRS test beam. Liu et al. (2020) similarly found that delamination and debonding of GFRP are crucial failure modes in reinforced concrete beams reinforced with GFRP. This research illustrates that delamination occurs because of excessive tensile stress in GFRP, resulting from the disparity in elastic moduli between GFRP and concrete [37, 38]. Furthermore, insufficient bonding between GFRP and concrete can also lead to delamination [39].

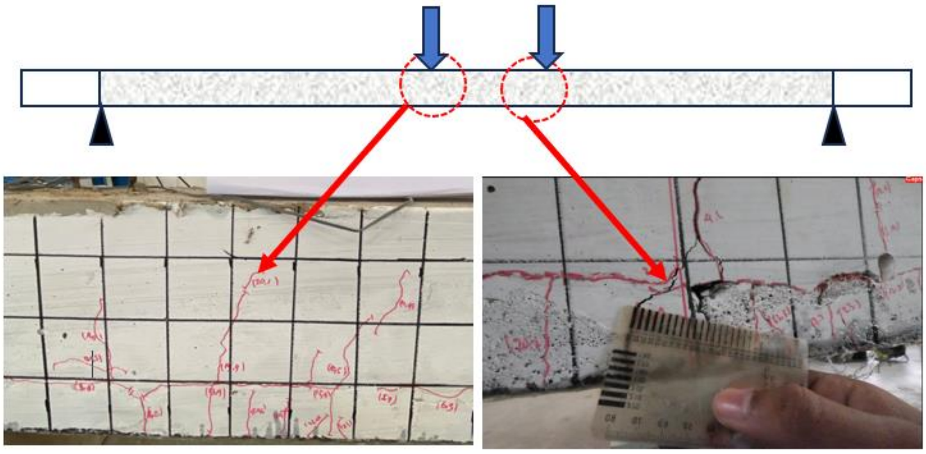

a. Early stage of fracture in BGRS b. Measurement of Crack Width

**Figure 13. BGRS beam damage measurement details**

As observed during the test (Figure 14), the initial flexural crack appeared in the BGRSF beam at a load of 5.53 kN, signaled by a faint crack sound that persisted as the load rose. Between the load range of 12.3 to 20.6 kN, this faint cracking sound intensified, particularly at the bottom of the beam in the region undergoing the maximum bending moment. The faint cracking sound may be linked to the release of residual stress in the concrete that has undergone the grouting process, as demonstrated in the research by Wu et al. (2022) [36]. At 20.6 kN load, tiny cracks appeared around the ends of the primary flexural crack, gradually spreading towards the compressive side of the beam. As the load increased to 30.3 kN, the sound of concrete cracking grew more pronounced. The extensive microcracking diminished the beam's stiffness and the cohesion between the concrete and GFRP. The microcracking continued to escalate until a sharp cracking sound was audible at 33.6 kN load. Upon reaching 33.85 kN load, debonding of GFRP occurred at a strain of 18424 με. Ultimately, the beam failed due to the compromised strength of GFRP, leading to the concrete fracturing in the middle span.

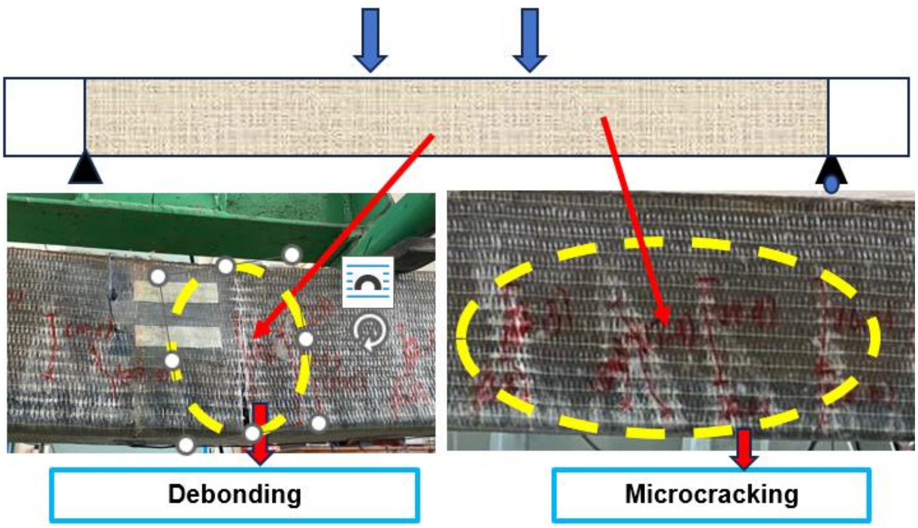


**Figure 14. Failure mode of Concrete Beam BGRSF**

The microcracks appearing at a load of 20.6 kN can be ascribed to the heightened tensile and shear stresses experienced by the GFRP, as demonstrated in the research by [18, 19]. The detachment of GFRP at 33.85 kN load marks a significant failure mode contributing to the beam's collapse. Multiple factors, including elevated tensile and shear stresses in GFRP and inadequate bonding between GFRP and concrete, can trigger GFRP debonding. Additional studies are required to explore the determinants influencing GFRP debonding. Moreover, research efforts should focus on devising strategies for GFRP reinforcement aimed at mitigating the likelihood of debonding.

## 4. Conclusions

From the experimental and analytical investigations conducted, the following conclusions can be inferred:

- The research investigated the structural ramifications of different repair and reinforcement techniques on reinforced concrete beams. Beams solely repaired through grouting (BGR) exhibited a notable decline in maximum load capacity, dropping by up to 51.6% compared to control beams (BK). Conversely, beams reinforced with GFRP strips (BGRS) demonstrated a modest increase in maximum load capacity, rising by 5.5% compared to BK beams. Beams entirely encased in GFRP (BGRSF) demonstrated the most significant enhancement in maximum load capacity, experiencing an 8.1% increase compared to BK beams. It's noteworthy that beams fully wrapped in GFRP exhibited superior performance, underscoring the potential efficacy of this approach in augmenting load-bearing capabilities.
- During flexural testing, distinct failure patterns emerged among the tested beams. BK beams displayed pure flexural failure at an average load of 29.74 kN, whereas BGR beams exhibited failure at a notably lower average load of 14.39 kN, primarily due to premature delamination. On the other hand, BGRS beams encountered flexural failure at 27.81 kN, attributed to delamination and debonding issues. In contrast, BGRSF beams demonstrated the highest ultimate average load of 32.14 kN, mainly due to debonding and microcracking. These outcomes highlight the effectiveness of GFRP reinforcement in augmenting the flexural capacity of reinforced concrete beams under post-spalling conditions.
- Post-repair assessment revealed notable alterations in flexural crack patterns. Initially, damaged beams primarily exhibited a single crack pattern in the zone of maximum moment. However, after grouting repair, there was an uptick in the variety of crack patterns, whereas beams reinforced with GFRP exhibited a decline in crack pattern frequency. This suggests structural improvement and underscores the importance of GFRP reinforcement in mitigating crack propagation and enhancing the overall integrity of reinforced concrete beams post-repair. These outcomes carry substantial implications for optimizing repair and reinforcement approaches in reinforced concrete structures to bolster their resilience and load-bearing capabilities.

## 5. Declarations

### 5.1. Author Contributions

Conceptualization: A.Z.N. and R.D.; methodology: H.P. and R.I.; software: A.Z.N.; validation: R.D., H.P., and R.I.; formal analysis: A.Z.N. and D.N.; investigation: A.Z.N.; resources: A.Z.N.; data curation: A.Z.N.; writing—original draft preparation: A.Z.N.; writing—review and editing: A.Z.N.; visualization: A.Z.N. and D.N.; supervision: R.D., H.P., and R.I.; project administration: A.Z.N. and D.N.; funding acquisition: A.Z.N. All authors have read and agreed to the final manuscript.

### 5.2. Data Availability Statement

The data presented in this study are available in the article.

### 5.3. Funding and Acknowledgements

We express our gratitude to the Center for Education Financial Services (PUSLABDIK) and the Indonesia Endowment Fund for Education (LPDP), under the Ministry of Education, Culture, Research, and Technology (RISTEKDIKTI) of the Republic of Indonesia, for their support.

### 5.4. Conflicts of Interest

The authors declare no conflict of interest.

## 6. References

[1] Jumaat, M. Z. Bin, Kabir, M. H., & Obaydullah, M. (2010). Structural performance of reinforced concrete beams repairing from spalling. European Journal of Scientific Research, 45(1), 89–102.

[2] Alwash, N. A., Kadhum, M. M., & Mahdi, A. M. (2019). Rehabilitation of corrosion-defected RC beam-column members using patch repair technique. Buildings, 9(5), 120. doi:10.3390/buildings9050120.

[3] Jung, J. S., Lee, B. Y., & Lee, K. S. (2019). Experimental Study on the Structural Performance Degradation of Corrosion-Damaged Reinforced Concrete Beams. Advances in Civil Engineering, 2019(1), 1-14. doi:10.1155/2019/9562574.

[4] Faroz, S. A., Ghosh, S., & Pushkaran, T. (2023). Optimum calibration of a corrosion rate instrument using information gain criterion within a Bayesian framework. Structural Safety, 104, 102354. doi:10.1016/j.strusafe.2023.102354.

[5] Wu, B., Cao, J. L., & Kang, L. (2018). End patch loading behavior and strengthening of locally corroded steel I-beams. Journal of Constructional Steel Research, 148, 371–382. doi:10.1016/j.jcsr.2018.05.029.

[6] Zhang, X., Zhang, Y., Liu, B., Liu, B., Wu, W., & Yang, C. (2021). Corrosion-induced spalling of concrete cover and its effects on shear strength of RC beams. Engineering Failure Analysis, 127, 105538. doi:10.1016/j.engfailanal.2021.105538.

[7] Altoubat, S., Maalej, M., & Shaikh, F. U. A. (2016). Laboratory Simulation of Corrosion Damage in Reinforced Concrete. International Journal of Concrete Structures and Materials, 10(3), 383–391. doi:10.1007/s40069-016-0138-7.

[8] Ghous Sohail, M., Wasee, M., Al Nuaimi, N., Alnahhal, W., & Hassan, M. K. (2022). Behavior of artificially corroded RC beams strengthened with CFRP and hybrid CFRP-GFRP laminates. Engineering Structures, 272, 114827. doi:10.1016/j.engstruct.2022.114827.

[9] Kioumarsi, M., Benenato, A., Ferracuti, B., & Imperatore, S. (2021). Residual flexural capacity of corroded prestressed reinforced concrete beams. Metals, 11(3). doi:10.3390/met11030442.

[10] Wu, Z., Yuan, H., Asakura, T., Yoshizawa, H., Kobayashi, A., Kojima, Y., & Ahmed, E. (2005). Peeling Behavior and Spalling Resistance of Bonded Bidirectional Fiber Reinforced Polymer Sheets. Journal of Composites for Construction, 9(3), 214–226. doi:10.1061/(asce)1090-0268(2005)9:3(214).

[11] Gergess, A. N., Shaikh Al Shabab, M., & Massouh, R. (2020). Repair of Severely Damaged Reinforced Concrete Beams with High-Strength Cementitious Grout. Transportation Research Record, 2674(6), 372–384. doi:10.1177/0361198120919116.

[12] Kim, H. Y., You, Y. J., & Ryu, G. S. (2021). Reinforced concrete slabs strengthened with carbon textile grid and cementitious grout. Materials, 14(17), 5046. doi:10.3390/ma14175046.

[13] Chen, C., Cai, H., & Cheng, L. (2021). Shear Strengthening of Corroded RC Beams Using UHPC–FRP Composites. Journal of Bridge Engineering, 26(1), 4020111. doi:10.1061/(asce)be.1943-5592.0001653.

[14] Focacci, F., D'Antino, T., & Carloni, C. (2024). Simplified Procedure to Determine the Cohesive Material Law of Fiber-Reinforced Cementitious Matrix (FRCM)–Substrate Joints. Materials, 17(7), 1627. doi:10.3390/ma17071627.

[15] Sleiman, E., Ferrier, E., Michel, L., & Saidi, M. (2024). Seismic behavior of masonry-infilled reinforced concrete frames strengthened using ultra-high performance concrete diagonal strips. Structures, 59, 105790. doi:10.1016/j.istruc.2023.105790.

[16] Jafarzadeh, H., & Nematzadeh, M. (2022). Flexural strengthening of fire-damaged GFRP-reinforced concrete beams using CFRP sheet: Experimental and analytical study. Composite Structures, 288, 115378. doi:10.1016/j.compstruct.2022.115378.

[17] Wu, W., He, X., Wu, C., He, J., & Yang, W. (2021). Fracture performance of GFRP-RC beams with working cracks in alkaline environment for eight years. Construction and Building Materials, 299. doi:10.1016/j.conbuildmat.2021.123757.

[18] Nguyen, T. H., Nguyen, V. T., Pham, X. D., Nguyen, M. H., & Le, P. L. (2024). Experimental Study on the Strengthening Effect of CFRP Sheets on Corrosion-Damaged, Eccentrically Loaded Reinforced Concrete Columns. International Journal of Civil Engineering, 22(4), 535-547. doi:10.1007/s40999-023-00911-8.

[19] Djamaluddin, R., Irmawaty, R., Hamzah, S., & Ngeljaratan, L. N. (2023). Effect of Bonding Area on Bond Stress Behavior of GFRP Bars in Concrete. Civil Engineering Journal, 9, 123-140. doi:10.28991/CEJ-SP2023-09-010.

[20] Ortega, I., Pellicer, T. M., Calderón, P. A., & Adam, J. M. (2018). Cement-based mortar patch repair of RC columns. Comparison with all-four-sides and one-side repair. Construction and Building Materials, 186, 338–350. doi:10.1016/j.conbuildmat.2018.07.148.

[21] Djamaluddin, R., & Irmawaty, R. (2017). Relationship Model of the Moment Capacity of GFRP Sheet Strengthened RC Beams to the Duration of Sea Water Exposure. Procedia Engineering, 180, 1195–1202. doi:10.1016/j.proeng.2017.04.280.

[22] Liu, M. (2023). Corrosion and Mechanical Behavior of Metal Materials. Materials, 16(3), 973. doi:10.3390/ma16030973.

[23] Mirdan, D., & Saleh, A. R. (2022). Flexural performance of reinforced concrete (RC) beam strengthened by UHPC layer. Case Studies in Construction Materials, 17, e01655. doi:10.1016/j.cscm.2022.e01655.

[24] Attari, N., Amziane, S., & Chemrouk, M. (2012). Flexural strengthening of concrete beams using CFRP, GFRP and hybrid FRP sheets. Construction and Building Materials, 37, 746–757. doi:10.1016/j.conbuildmat.2012.07.052.

[25] Saribiyik, A., & Caglar, N. (2016). Flexural strengthening of RC beams with low-strength concrete using GFRP and CFRP. Structural Engineering and Mechanics, 58(5), 825–845. doi:10.12989/sem.2016.58.5.825.

[26] Oh, H. S., & Sim, J. (2004). Interface debonding failure in beams strengthened with externally bonded GFRP. Composite Interfaces, 11(1), 25–42. doi:10.1163/156855404322681037.

[27] Almusallam, T. H. (2006). Load-deflection behavior of RC beams strengthened with GFRP sheets subjected to different environmental conditions. Cement and Concrete Composites, 28(10), 879–889. doi:10.1016/j.cemconcomp.2006.07.017.

[28] Zhao, J., Luo, X., Wang, Z., Feng, S., Gong, X., & Shumuye, E. D. (2021). Experimental study on bond performance of carbon- and glass-fiber reinforced polymer (CFRP/GFRP) bars and steel strands to concrete. Materials, 14(5), 1–22. doi:10.3390/ma14051268.

[29] Stanciu, M. D., Drăghicescu, H. T., & Roșca, I. C. (2021). Mechanical properties of GFRPs exposed to tensile, compression and tensile—tensile cyclic tests. Polymers, 13(6), 898. doi:10.3390/polym13060898.

[30] Araby, M. Z., Rizal, S., Abdullah, Afifuddin, M., & Hasan, M. (2022). Deformation Capacity of RC Beam-Column Joints Strengthened with Ferrocement. Sustainability (Switzerland), 14(8), 4398. doi:10.3390/su14084398.

[31] Al-Asadi, A. K. (2019). Application of external prestressing on the rehabilitation of reinforced concrete beams. Periodicals of Engineering and Natural Sciences, 7(3), 974–984. doi:10.21533/pen.v7i3.630.

[32] Djamaluddin, R., Amir Sultan, M., Irmawati, R., & Shinichi, H. (2015). Bond Characteristics of GFRP Sheet on Strengthened Concrete Beams due to Flexural Loading. International Journal of Engineering and Technology, 7(2), 110–115. doi:10.7763/ijet.2015.v7.776.

[33] Mahmood, E. M., Allawi, A. A., & El-Zohairy, A. (2022). Flexural Performance of Encased Pultruded GFRP I-Beam with High Strength Concrete under Static Loading. Materials, 15(13), 4519. doi:10.3390/ma15134519.

[34] Naser, M. Z., Hawileh, R. A., & Abdalla, J. A. (2019). Fiber-reinforced polymer composites in strengthening reinforced concrete structures: A critical review. Engineering Structures, 198, 109542. doi:10.1016/j.engstruct.2019.109542.

[35] Kim, J., Jeong, S., Kim, H., Kim, Y., & Park, S. (2022). Bond Strength Properties of GFRP and CFRP according to Concrete Strength. Applied Sciences (Switzerland), 12(20), 10611. doi:10.3390/app122010611.

[36] Wu, C., Su, Y., Zhang, P., Zhu, H., Gao, D., & Sheikh, S. A. (2022). Experimental Study of GFRP Reinforced Concrete Beams With U-Shaped CFRP Grid-Reinforced ECC Stay-in-Place Formwork. Frontiers in Materials, 9. doi:10.3389/fmats.2022.872232.

[37] Abbas, H., Elsanadedy, H., Alaoud, L., Almusallam, T., & Al-Salloum, Y. (2023). Effect of confining stirrups and bar gap in improving bond behavior of glass fiber reinforced polymer (GFRP) bar lap splices in RC beams. Construction and Building Materials, 365, 129943.

[38] Hijriah, Parung, H., Djamaluddin, R., & Irmawaty, R. (2019). Study on Behavior of FRP Sheet Debonding As Flexural Strengthening of Reinforced Concrete Beam. International Journal of Civil Engineering and Technology, 10(09), 252–260.

[39] Liu, R., Cheng, Z., Yang, S., Zhang, P., Hu, Y., & Ye, N. (2023). Experimental study on the performance of shear connections between local UHPC slabs and GFRP girders. Structures, 55, 1966–1979. doi:10.1016/j.istruc.2023.05.090.